Journal of Marine Systems 88 (2011) 102–112

Contents lists available at ScienceDirect

Journal of Marine Systems

journal homepage: www.elsevier.com/locate/jmarsys

Long-term evolution of nourished beaches under high angle wave conditions

Niels van den Berg *, Albert Falqués, Francesca Ribas

Applied Physics Department, Universitat Politècnica de Catalunya, Spain

ARTICLE INFO

Available online 1 March 2011

Keywords:
Alongshore sediment transport
Beach morphology
Beach nourishment
Coastline instability
High angle waves
Shoreline sand waves

ABSTRACT

A nonlinear numerical model for large-scale dynamics of shoreline and nearshore bathymetry under wave action is applied to investigate the long-term evolution of a rectilinear coast dominated by high angle wave incidence, which is perturbed by a nourishment or an offshore borrow pit. Previous studies show that a coastline can be unstable due to high angle wave instability, which results from the feedback between shoreline changes and the wave field. In contrast to traditional one-line shoreline models, which always predict a diffusional behaviour, this instability can lead to the growth of shoreline perturbations. Model results suggest that due to high angle wave instability a nourishment or a borrow pit could trigger the formation of a shoreline sand wave train (alternating accretional and erosional zones). Its formation is a self-organised response of the morphodynamic system and can be seen as a spatial-temporal instability. New sand waves are formed downdrift while the old sand waves migrate downdrift and increase in amplitude and wavelength. Instability develops only if the bathymetric changes related to shoreline perturbations extend to a depth where the wave angle is greater than the critical angle of 42°. The potential for coastline instability is therefore limited by the wave incidence angle at the depth of closure and not the angle at deep water as suggested in previous studies. Including a fraction of low angle waves to the wave climate causes saturation of the amplitudes of the sand waves and limits the formation of the sand wave train. Even on a stable coast dominated by low angle waves, the feedback between morphology and the wave field can be crucial for the prediction of nourishment evolution. This feedback leads to relatively slow diffusion of shoreline perturbations and it can lead to downdrift migration. While some existing observations describe downdrift advection, no satisfactory explanation had been provided previously.

1. Introduction

Shore nourishment is used in coastal engineering to mitigate beach erosion. The nourishment can be seen as a perturbation of the dynamic equilibrium of the coastline and since this perturbation is eventually diffused in cross-shore and alongshore directions, nourishment is considered to be a temporary solution. When a net alongshore transport is present, the perturbation can also undergo advection (Hamm et al., 2002).

Within the process of nourishment design and planning, modelling plays an important role. Capobianco et al. (2002) gave an extensive review of different shoreline change models and their applicability on nourishment planning. The increasing understanding of nearshore dynamics has lead to the development of detailed process-based models. These models however still have a low skill in predicting shoreline dynamics. Furthermore they require detailed field data for calibration and they are computationally demanding. Therefore, simple one-line shoreline change models are commonly used for long-term and large-scale simulations. These models are based on the assumption that shoreline changes are caused by gradients in wave driven alongshore (Komar, 1998; Dean, 2002). This alongshore transport is commonly computed with the empirical CERC formula, which relates alongshore transport with the wave height at breaking (H_b) and the angle between the wave fronts and the shoreline orientation ($\theta_b - \phi$), where θ_b is the wave incidence angle at breaking with respect to the shore normal and ϕ is the angle between the local shoreline and the mean rectilinear shoreline. When this approach is applied to small amplitude changes on a rectilinear coastline the Pelnard–Considère equation for the shoreline position can be derived (Pelnard-Considère, 1956). This is a diffusion equation, which predicts a stable coastline and the diffusion of perturbations of the shoreline. The diffusivity coefficient in this equation is called coastline diffusivity. This concept can also be applied in a more general context and the coastline diffusivity can be estimated as the squared length scale of a perturbation divided by its decay time.

In recent years it has been demonstrated that when the wave climate is dominated by high angle waves this situation can be reversed and the coastline becomes unstable (actually, this was previously suggested by Zenkovich (1959)). This instability of the coastline will be referred to as high angle wave instability (from now on called HAWI). Ashton et al. (2001) used a non-linear cellular model

* Corresponding author at: Departament de Física Aplicada, Universitat Politècnica de Catalunya, Campus Nord, Edifici B4/B5, C/ Jordi Girona Salgado 1-3, 08034, Barcelona, Spain.
E-mail address: niels@fa.upc.edu (N. van den Berg).

0924-7963/$ – see front matter © 2011 Elsevier B.V. All rights reserved.
doi:10.1016/j.jmarsys.2011.02.018

to explore HAWI. They found that small perturbations on a rectilinear coastline can grow and migrate if the incidence angle of offshore waves with respect to the shore normal (θ_0) is higher than a critical value of 42°. Non-linear effects made the largest perturbations to dominate and they reproduced large scale coastal patterns resembling shoreline sand waves, capes and spits Ashton and Murray (2006a). In the present study we use the term shoreline sand wave field to refer to an undulating shoreline with alternating accretional and erosional zones, like the pattern described by Ashton and Murray (2006a). Falqués (2003) showed that HAWI is the result of the feedback of the shoreline changes into the wave field, a feedback ignored in the traditional one-line models. When shoreline variations extend into the nearshore bathymetry they affect wave transformation. Work and Rogers (1997) and Thevenot and Kraus (1995) already included the effect of wave refraction in their shoreline models, leading to a lower θ_b and a reduction of the coastline diffusivity. The reduction of the coastline diffusivity maybe up to about 50% (Dean, 2002). Refraction also leads to alongshore gradients in H_b through wave energy spreading and focusing. Ashton and Murray (2006b) and Falqués et al. (2011) suggested that it is wave energy spreading that is essential for HAWI. For θ_0 lower than 42°, alongshore gradients in $\theta_b - \phi$ are dominant for alongshore transport and the resulting transport pattern leads to diffusion of shoreline perturbations. For θ_0 greater than 42°, gradients in H_b at breaking become dominant for the alongshore transport and this leads to a different transport pattern, enabling a perturbation to grow and migrate.

List and Ashton (2007) confirmed that a shoreline can potentially be unstable for high angle wave conditions by modelling initial transport gradient patterns with the use of a fully 2DH process-based wave, circulation and sediment transport model. Some discussion exist about the capacity of the CERC formula to correctly predict gradients in alongshore sediment transport that result from wave transformation over bathymetric perturbations (List et al., 2006, 2008). However, the results of List and Ashton (2007) suggest that the CERC formula predicts qualitatively correct transport gradients along large scale shoreline undulations (alongshore lengths of 1–8 km).

The two main limitations of the studies by Ashton and Murray (2006a,b) and Falqués (2003) are that the bathymetric lines are rectilinear and that the perturbations of the shoreline extend offshore in the bathymetry to infinite distance. Falqués and Calvete (2005) developed an one-line model with curvilinear bathymetric lines and a finite extension of the perturbations in the cross-shore direction. They used linear stability analysis to explore the HAWI mechanism. The model was able to predict instability and the formation of a shoreline sand wave field. They found that if the bathymetric perturbation is confined close to the shoreline, no instability develops. This enlightens the importance of cross-shore profile dynamics for the HAWI mechanism. They found typical initial growth times of 1–10 years and wavelengths in the order of 4–15 km for the modelled sand wave field. Since this study used a linear approach it was only valid for small amplitude perturbations. A second limitation was that the cross-shore extension of the perturbation was fixed in time.

In the present study an extension of the one-line model used by Falqués and Calvete (2005) is presented. This model, called Q2D-Morfo, is non-linear, can simulate large amplitude perturbations and treats the cross-shore extension of the perturbations as finite and dynamic. The aim of this study is to understand the long term evolution of nourished beaches under high angle wave conditions. It is expected that, under these conditions, a nourishment can act as a perturbation that triggers shoreline instability and the growth of shoreline sand waves. Two different nourishment scenarios are used for the numerical simulations, a beach nourishment and a shoreface nourishment. A third scenario used is a straight coastline with the presence of a nearshore dredge pit. The three scenarios are expected to respond differently to high angle wave conditions. The influence of the offshore wave conditions and nourishment dimensions on the shoreline evolution are also studied.

2. Nourishment methods and shoreline response

The most traditional nourishment method is beach nourishment. This involves the placement of large quantities of sand on the sub-aerial beach, advancing the shoreline seaward (Dean, 2002). The volume of sand involved in beach nourishment is in the range of one to several million cubic meters spread over an alongshore section of several kilometers. The shoreline advances seaward several tens of meters and the initial nourished cross-shore profile is usually steeper than the original beach profile. This often results in an initially rapid diffusion in cross-shore direction until the equilibrium shape of the profile is restored. The planform diffusion depends on wave conditions and the amplitude and length of the nourishment. Typically the diffusion is slower for a long nourishment with a small amplitude. Grove et al. (1987) suggested that apart from diffusing a beach nourishment can initiate a solitary downdrift migrating shoreline sand wave, i.e. a single accretional zone (crest) sometimes followed by an erosional zone (trough). This suggestion is supported by various studies on other sites where the input of a large body of sand to a coastline appears to initiate a shoreline sand wave. The input of sand can be due to nearshore bar welding (Davidson-Arnott and van Heyningen, 2003), episodic inlet opening (Thevenot and Kraus, 1995), sediment bypass pulses at inlets (Ruessink and Jeuken, 2002) and riverine flood deposits (Inman, 1987). When these natural inputs of sediments are periodic they could lead to the initiation of multiple shoreline sand waves.

A second nourishment approach is shoreface nourishment, in which the sand is placed as a submerged berm (Dean, 2002). The submerged berm is located within the active zone of the cross-shore profile over an alongshore section of several kilometres. This method is gaining popularity as it seems to be effective and is cheaper than beach nourishment. Its effectiveness depends on two mechanisms. The first one is the feeder effect due to onshore transport of sand from the shoreface nourishment to the beach. The second one is the lee effect of the berm, which causes wave shadow and wave focusing leading to gradients in alongshore sediment transport. In particular, when a net alongshore transport is present there will be accretion in the lee of the berm due to a decrease in transport capacity. This can however also cause a down drift zone of erosion due to the subsequent increasing transport capacity (van Duin et al., 2004). The behaviour of shoreface nourishments is usually complex as they interact with bar dynamics (Grunnet and Ruessink, 2004).

Nourishments require a nearby source of good quality sand, which is usually dredged from an offshore location. These borrow pits can affect the shoreline directly by trapping sediment from the nearshore and indirectly through wave transformation and the resulting transport gradients (Dean, 2002). Borrow pits are generally located at depths greater than the depth of closure (D_c). Therefore they fill in very slowly and their forcing on the shoreline can persist for decades. As it has been mentioned in Section 1, there exists some discussion on the capacity of the CERC formula to correctly predict transport gradients due to bathymetric perturbations like borrow pits. On the one hand, Bender and Dean (2004) used an analytical wave transformation and the CERC formula to compute alongshore sediment transport and their predictions showed accretion in the shadow zone of a borrow pit with a downdrift erosional zone, qualitatively in agreement with results of process based models (Benedet and List, 2008; Hartog et al., 2008). These results were only obtained if an additional term, which describes the contribution of alongshore gradients in wave height (Ozasa and Brampton, 1980), was added to the CERC formula. On the other hand, List et al. (2006, 2008) suggested that the transport gradients shoreward of a borrow pit computed with the CERC formula are out of phase with those of a

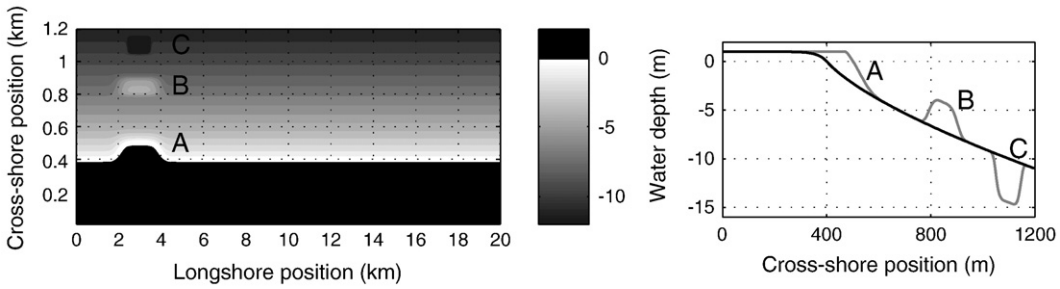

Fig. 1. Initial bathymetry (left panel) and cross-shore transect at $y=3$ km (right panel) showing the three possible nourishment scenarios: beach nourishment (A), shoreface nourishment (B), and borrow pit (C).

process based model even when the additional term is added to the CERC formula. Probably, the validity of the CERC formula in the context of bathymetric perturbations depends largely on their length scale. Therefore care should be taken when the CERC formula is used to predict alongshore transport gradients changes shoreward of a borrow pit when no observations are available for calibration.

3. Model

The Q2D-morfo model is a non-linear morphodynamic model developed to simulate large-scale shoreline dynamics. It considers sediment transport in two horizontal dimensions and computes the wave field over the whole domain. Convergence and divergence of sediment transport lead to bathymetric changes which feedback to the wave field in the next time step. A Cartesian frame with horizontal coordinates x, y and vertical coordinate z is used, where y is along the initial mean shoreline orientation. The unknowns are the moving shoreline $x=x_s(y,t)$ and the changing bed level $z=z_b(x,y,t)$.

The dynamic equation for the bed level is the sediment mass conservation,

$$\frac{\partial z_b}{\partial t}+\frac{\partial q_x}{\partial x}+\frac{\partial q_y}{\partial y}=0, \tag{1}$$

where $\vec{q}=(q_x,q_y)$ is the depth integrated sediment flux with the bed porosity factor included. This equation is discretized by using an explicit second order Adam–Bashfort scheme in time and a finite difference method in space.

3.1. Sediment transport

The sediment transport is computed directly from the wave field via parametrisations. This simplification is common for one-line and N-line models and it allows simulations for large spatial and temporal scales. Small scale surf zone dynamics can however not be reproduced. The total sediment flux is the sum of three terms,

$$\vec{q}=\vec{q}_l+\vec{q}_c+\vec{q}_d. \tag{2}$$

The first term in Eq. (2) represents the wave driven alongshore transport. First, the cross-shore integrated sediment transport rate is computed with an extended version of the CERC formula (Komar, 1998). The formula has been adapted to include a second term introduced by Ozasa and Brampton (1980), which represents the contribution of alongshore gradients in wave height to the alongshore transport,

$$Q_l=\mu H_b^{\frac{5}{2}}\left(sin(2\alpha_b)-\frac{2r}{\beta}cos(\alpha_b)\frac{\partial H_b}{\partial y}\right), \tag{3}$$

where $H_b(y)$ is the root mean square wave height at breaking, $\alpha_b=\theta_b(y)-\phi(y)$ is the angle between the wave fronts at breaking and the coastline and β is the local swash slope. The constant μ is proportional to the empirical parameter K_1 of the original CERC formula. This model parameter controls the magnitude of the transport and the default value of $\mu=0.2m^{0.5}s^{-1}$ corresponds to $K_1=0.7$. The constant $r=K_2/K_1$, where K_2 is the empirical parameter of the second term (Ozasa and Brampton, 1980). The default value used is $r=1$, which is equivalent to $K_2=K_1$, the value used by Bender and Dean (2004).

The sediment flux q_l is computed as follows,

$$\vec{q}_l=f(x)Q_l(y)(sin\phi,cos\phi), \tag{4}$$

where $f(x)$ is a cross-shore distribution function, qualitatively based on the cross-shore profile of the longshore current (Komar, 1998),

$$f(x)=\frac{4}{\sqrt{\pi}L^3}x^2e^{-(x/L)^2}, \tag{5}$$

where $L=0.7X_b(y)$ and $X_b(y)$ is the width of the surfzone. The orientation of the coastline $\phi(y)$ is not the angle of the shoreline relative to the y-axis but the mean orientation of the bathymetric lines within the surf zone with respect to the y-axis. This is the orientation felt by the breaking waves. The angle $\phi(y)$ is determined by computing the average orientation within a rectangle with dimensions equal to the surf zone width.

The second term in Eq. (2) is a parametrisation of cross-shore sediment transport processes. We assume that, on a relatively long time scale, these processes drive the cross-shore profile to an equilibrium profile z_{be}, so that

$$\vec{q}_c=-\gamma_x\left(\frac{\partial(z_b-z_{be})}{\partial x}\right)(1,0), \tag{6}$$

where γ_x is a cross-shore diffusivity coefficient. The third term in Eq. (2) is an alongshore diffusivity (in the direction of the

Table 1
Geometric characteristics of the three nourishment scenarios.

Scenario	Length	Bed level	Volume
Beach nourishment	2 km	1 to −4 m	0.68 Mm^3
Shoreface nourishment	2 km	−6 to −8 m	0.65 Mm^3
Borrow pit	1 km	−9 to −11 m	0.43 Mm^3

Table 2
Offshore wave conditions: default value and range of variation.

Parameter	Default	Range
θ_0	60°	20 − 70°
H_0 (rms)	1 m	0.5–1.5 m
T_p	6 s	4–8 s

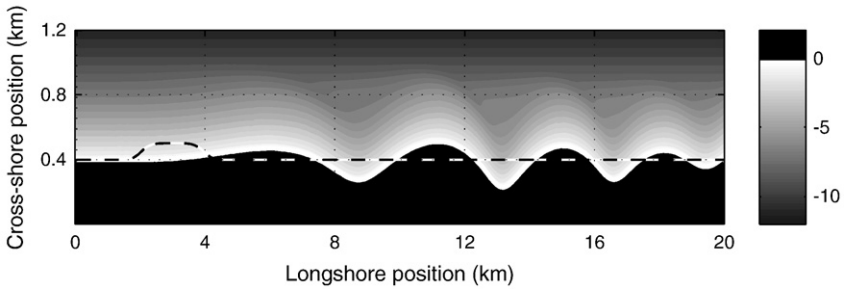

Fig. 2. Bathymetry after 8 years for the beach nourishment scenario and the default offshore wave conditions. The dotted line represents the initial shoreline with the beach nourishment. Notice the exaggeration in the cross-shore axis.

surfzone contour lines) that suppresses the growth of small scale noise,

$$\vec{q}_d = -\gamma_y\left(\frac{\partial z_b}{\partial x}sin\phi + \frac{\partial z_b}{\partial y}cos\phi\right)(sin\phi, cos\phi). \quad (7)$$

The physical basis for the coefficients γ_x and γ_y is the diffusivity caused by wave breaking. Thereby, they depend on the wave energy dissipation and their order of magnitude has been estimated by using the expression for momentum mixing due to wave breaking,

$$\nu_t = M(\mathcal{D}/\rho)^{1/3}H, \quad (8)$$

where M is a nondimensional constant, $\mathcal{D}$ is the wave energy dissipation per time and area unit, ρ is the water density and H is the root mean square wave height. We assume that γ_x and γ_y scale with ν_t. The order of magnitude of $\mathcal{D}$ can be estimated as the total energy flux entering the surfzone divided by the area,

$$\mathcal{D} \sim \frac{1}{8}\rho g H_b^2 \frac{c_{gb}}{X_b}, \quad (9)$$

where g is the gravity acceleration and c_{gb} is the group celerity at breaking, computed with the shallow water assumption. An estimation for the morphodynamic diffusivity is therefore,

$$\gamma_x(x,y) = \epsilon_x \gamma_b^{-1/6} g^{1/2} H_b^{11/6} X_b^{-1/3}\psi(x) \quad (10)$$

where ϵ_x is a nondimensional constant and γ_b is the breaking index (the ratio wave height to water depth at breaking). The shape function $\psi(x)$ has a cross-shore distribution with a maximum in the surf zone and decays to almost zero at the depth of closure, D_c.

This cross-shore distribution function depends on the wave height and the position of the shoreline. Higher waves and an offshore moving shoreline shift D_c offshore. A similar expression is used for $\gamma_y(x,y)$, with a coefficient ϵ_y.

Table 3
Sand wave train characteristics after 8 years for the three nourishment scenarios and the default offshore wave conditions, where σ is the standard deviation of the shoreline, λ is the wavelength, a_c is the amplitude of the crest, a_t is the amplitude of the trough and the subscripts refer to the first to fourth sand wave.

Parameter	Beach	Shoreface	Borrow
σ (m)	63	98	118
λ_1 (km)	7.2	7.0	7.5
a_{c1} (m)	67	111	145
a_{t1} (m)	131	208	226
λ_2 (km)	4.2	4.6	5.6
a_{c2} (m)	105	155	190
a_{t2} (m)	157	253	262
λ_3 (km)	3.3	3.2	3.3
a_{c3} (m)	80	95	109
a_{t1} (m)	107	160	102
λ_4 (km)	2.6	2.4	2.3
a_{c4} (m)	51	64	63
a_{t4} (m)	44	41	76

3.2. Wave module

The wave height H_b and angle θ_b at breaking are needed for the computation of the sediment transport. The wave module computes the wave field from the wave height, period and angle given at the offshore boundary, based on the following equations,

$$\omega^2 = gk\,tanh(kD), \quad (11)$$

$$\frac{\partial k_y}{\partial x} = \frac{\partial k_x}{\partial y}, \quad (12)$$

$$\frac{\partial}{\partial x}\left(c_g H^2 \frac{k_x}{k}\right) + \frac{\partial}{\partial y}\left(c_g H^2 \frac{k_y}{k}\right) = 0, \quad (13)$$

where $\omega = 2\pi/T_p$ is the radian frequency, T_p is the peak period, $\vec{k} = \left(k_x, k_y\right) = k(-cos\theta, sin\theta)$ is the wave number vector, D is the water depth, c_g is the group celerity and θ is the wave crest angle with respect to the x-axis. Eq. (11) is the dispersion relation, Eq. (12) is the equation for wave number irrotationality and Eq. (13) is the wave energy conservation. Dissipation by bottom shear stresses is neglected and dissipation by breaking is not included because the wave field is only needed up to breaking. The point of breaking is defined as $H = \gamma_b D$, where γ_b is the breaking index.

3.3. Boundary conditions

At the shoreline the following condition is used,

$$\vec{q}(x = x_s) = \gamma_s\left(\frac{\partial z_b}{\partial x}cos\phi_s - \frac{\partial z_b}{\partial y}sin\phi_s - \beta_s\right)(cos\phi_s, -sin\phi_s), \quad (14)$$

where ϕ_s is the angle between the shoreline and the y-axis, β_s is an equilibrium slope and γ_s is the swash zone diffusivity coefficient. This equation simulates the relaxing of the swash slope to an equilibrium slope. If the swash slope is smaller than the equilibrium slope, sediment is transported from the wet cells to the dry cells and the shoreline advances seaward. If the swash slope is steeper, the dry beach is eroded and the shoreline retreats. The coefficient γ_s is related to the swash zone relaxation time T_s by $\gamma_s \sim (\Delta x)^2/T_s$, where Δx is the grid size and T_s is of the order of a few hours. At the seaward boundary the sediment flux consists of a residual diffusive cross-shore transport calculated by assuming that the profile relaxes to the equilibrium profile within a decay distance λ from the boundary. At the lateral boundaries there is no diffusive transport and only wave driven alongshore transport is considered.

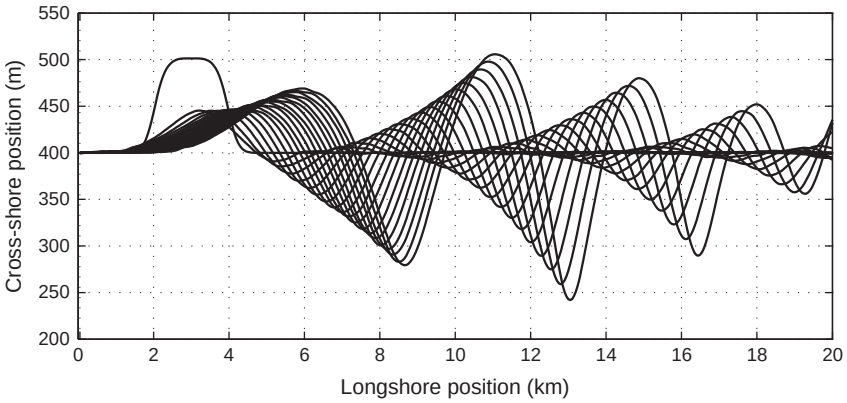

Fig. 3. Time evolution of the shoreline for the beach nourishment scenario and default offshore wave conditions. The shoreline is plotted every 6 months and the final line corresponds to the result after 8 years. Notice the exaggeration in the cross-shore axis.

4. Methodology

4.1. Model setup and numerics

The modelled domain is a 20 km long stretch of beach with a cross-shore width of 1.2 km (Fig. 1). The dry beach is 400 m wide and a Dean shaped profile is used as the equilibrium cross-shore profile,

$$Z(x) = -A\Big((x+d)^{2/3} - d^{2/3}, \tag{15}$$

where d introduces a small shift to avoid an infinite slope at the shoreline. The constants d and A are determined by prescribing the swash slope at the shoreline ($\beta = 0.03$) and the water depth at the offshore boundary ($D_o = 11$ m). The equilibrium profile z_{be} used in Eq. (6) is determined as $z_{be} = Z(x - x_s)$. A grid with a cell size of 50 m alongshore and 5 m cross-shore is used. Model parameter μ, controlling sediment transport rates is set to a default value of $0.2\, m^{\frac{1}{2}} s^{-1}$. The cross-shore diffusivity coefficient, ϵ_x, is set to 0.05, based on a realistic cross-shore response time. ϵ_y is also set to 0.05 and γ_s is set to 0.001 m^2/s. A cross-shore distribution profile is chosen so that $D_c = 7$ m for default wave conditions. The breaking index γ_b is set to an intermediate value of 0.5. A time-step of 0.001 days is used to satisfy the Courant numerical stability condition and the wave field is computed every day.

4.2. Nourishment scenarios

The location and dimensions of the three nourishment scenarios can be found in Table 1 and Fig. 1. The nourishments are placed 3 km from the updrift boundary. The beach nourishment is 2 km long and advances the shoreline 100 m. The foot of the beach nourishment is located at 4 m depth and the cross-shore slope of the perturbation is steeper than the equilibrium slope. To study the effect of the dimensions of the beach nourishment, simulations with half and double the alongshore length of the beach nourishment are also done. The shoreface nourishment is located between the −6 and −8 m bed level contours and has a height of 3 m. The water depth above the crest of the shoreface nourishment is 4 m. The borrow pit is 1 km long and 100 m wide. It is located between the −9 and −11 m bed level contours and it has a depth of 4 m.

4.3. Wave conditions

Various wave conditions are imposed at the offshore boundary (Table 2). The waves are unidirectional and the wave height and period are constant during each simulation. The range of realistic wave angles that can be considered at the offshore boundary has an upper limit, which depends on the water depth and wave period. Before reaching the offshore boundary the incident waves refract over straight bathymetric lines. Incidence angles will therefore be lower for long period waves and small water depth at the offshore boundary. For example, the maximum realistic wave angle for waves with a period of 6 seconds and an offshore water depth of 11 m is 65°.

4.4. Alternative model setup

In the default simulations the model is fully dynamical and wave refraction is computed over the changing bathymetry. This results in gradients in θ_b and H_b, which lead to divergence and convergence of alongshore transport and changes in the shoreline. Other model setups are used in order to identify the direct effect of wave refraction and indirect effect on H_b, due to wave energy spreading and focusing, on the evolution of a shoreline perturbation. In these setups the alongshore gradients of θ_b and H_b are artificially disconnected separately. The simulations are done for the beach nourishment scenario and two offshore wave incidence angles are used, $\theta_0 = 40°$ and $\theta_0 = 60°$.

4.5. Instability criterion

According to Ashton et al. (2001) a coastline is potentially unstable if deep water waves are dominated by incidence angles greater than 42° (θ_{cr}). This is only valid if it is assumed that the shoreline perturbation extends in the bathymetric lines up to infinity. In the present study we assume that perturbations are finite and dynamic. The maximum possible extension of the shoreline perturbations is until D_c. This is the maximum depth at which the bathymetric perturbations can affect the wave field. Therefore, it is the wave incidence angle at D_c (θ_{Dc}) that should be compared with θ_{cr}. A coastline is potentially unstable in case the dominant wave incidence angle at D_c is greater than 42° ($\theta_{Dc} > \theta_{cr}$).

5. Results

5.1. Beach nourishment evolution for default conditions

Fig. 2 shows the bathymetry and shoreline position after a simulation of 8 years with default conditions. The beach nourishment clearly triggered the growth of a shoreline sand wave train. This was expected for these default conditions because θ_{Dc} was about 50° and the coastline was potentially unstable. The initial perturbation was partly diffused and migrated downdrift. Together with its downdrift erosional zone the first crest can be seen as a sand wave with a wavelength λ_1 of 7.2 km. The wavelength is measured from the updrift beginning of the crest until the downdrift end of the trough.

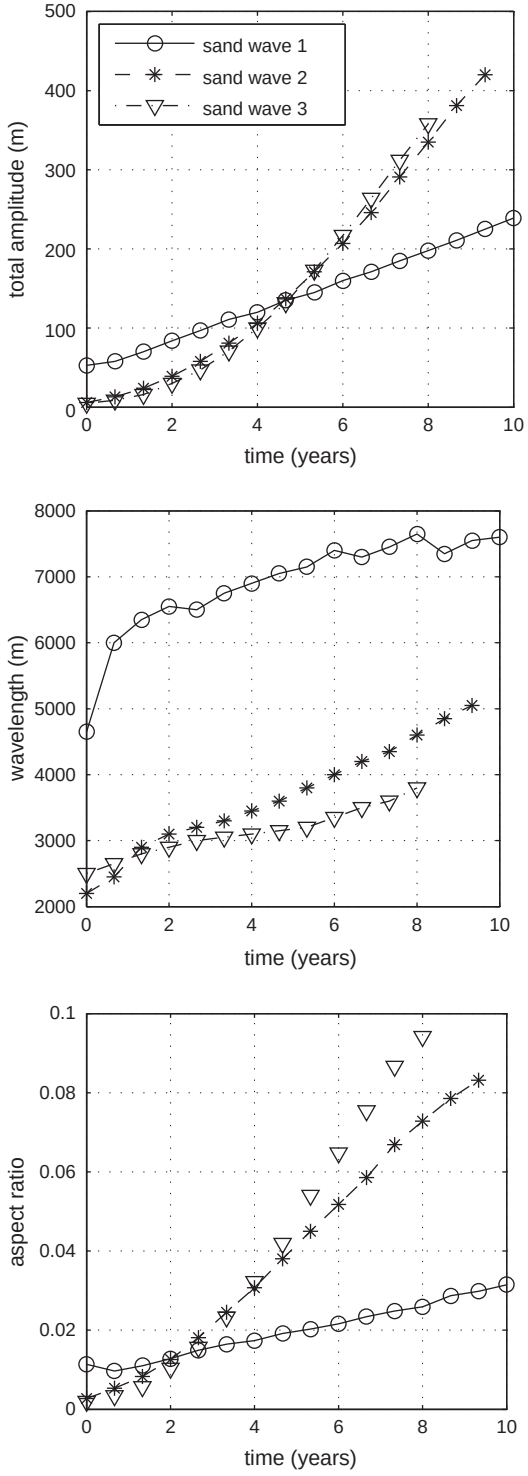

Fig. 4. The evolution of the total amplitude (crest to trough), the wavelength and the aspect ratio (total amplitude divided by wavelength) for the beach nourishment scenario and default wave conditions. The 3 lines represent the first to third sand waves of the sand wave train.

The amplitude of the crest, a_{c1}, is 67 m and the amplitude of the trough, a_{t1}, is 131 m. Table 3 shows the characteristics of the three oscillations of the sand wave train. The standard deviation σ of the shoreline, used as a simple measure for sand wave development, is 63 m. Notice that σ does not give information about the actual patterns on the shoreline and when the domain gets saturated with a sand wave field the generation of new sand waves outside the domain does not contribute anymore to its value.

In Fig. 3 the evolution of the shoreline over 8 years can be seen with time intervals of half a year. The evolution can be split in two different processes, the evolution of the initial perturbation and the evolution of the triggered downdrift sand wave train. The first process took place during the first year and can be summarised as follows: a) diffusion of the initial perturbation, mainly in cross-shore direction, b) downdrift migration of the crest, c) development of asymmetry, d) development of a downdrift erosional zone, and e) growth in amplitude of the crest and the trough. The second process can be summarised as follows: a) triggering of the growth of a downdrift crest by the erosional zone, b) growth of this second crest, and c) triggering of a second downdrift erosional zone. This feedback process continued during the 8-year period until three sand waves developed within the domain. The growth in total amplitude (crest to trough) and the wavelengths of the second and third sand waves were similar (Fig. 4). The amplitude increased faster than the wavelength so that the aspect ratio (total amplitude divided by wavelength) increased in time. The aspect ratio of the first sand wave was much lower. The increase of the aspect ratio seems to slow down at the end of the simulation but it is not clear if a constant aspect ratio would be attained as in Ashton and Murray (2006a). A longer simulation time was not possible because non-linear behaviour led to abrupt bathymetric changes in the troughs of the sand waves, resulting in a crash of the model.

The migration rate of the sand waves is evaluated every 6 months by dividing the distance travelled by the crest and trough by time. The migration rates of all the sand waves attained a constant value 4 years after their generation. The initial perturbation migrated downdrift with an average rate of about 340 m/yr and the second and third sand waves with respectively 580 m/yr and 780 m/yr. The migration rate was higher for each subsequent downdrift sand wave, which is consistent with the increase in wavelength of the updrift sand waves. Also, the trough of the sand waves in general migrated faster than the corresponding crest.

Two simulations with half and double alongshore length of the beach nourishment, respectively, were also performed. The initial sand wave that directly develops from the nourishment grew to a larger amplitude and wavelength in case of a longer nourishment. However, the results suggest that the dimensions of the nourishment do not influence the characteristics of the sand wave train.

5.2. Shoreface nourishment and borrow pit evolution for default conditions

The shoreline evolution in the other two scenarios were compared with the beach nourishment scenario (Fig. 5 and Table 3). In general the beach and shoreface nourishment evolved in a similar way, however the latter resulted into greater amplitudes of the sand waves. The shoreface nourishments first forced the growth of a shoreline perturbation due to the transport gradients appearing in its shadow. The larger amplitude of the first sand wave can be explained by the prolonged forcing on the shoreline by the shoreface nourishment. After 2 years the shoreface nourishment had diffused and from that moment on the shoreline dynamics were only controlled by the feedback between the shoreline changes and the wave field, just as for the beach nourishment scenario. The borrow pit scenario showed a different behaviour. The crest of the first sand wave remained at the same location and only grew in amplitude. The resulting downdrift erosional zone was limited in its downdrift migration by the stationary crest but it was sufficient to increase the wavelength of the first sand wave. The combination of the static position of the crest and the sedimentation in the trough led to a bumpy shape. Two phases of the time evolution can be distinguished in Fig. 6. For the borrow pit scenario σ shows an initial fast growth and, after 2 years, it increases linearly with time. These first 2 years can be seen as the initial phase which includes the initial perturbation of the shoreline

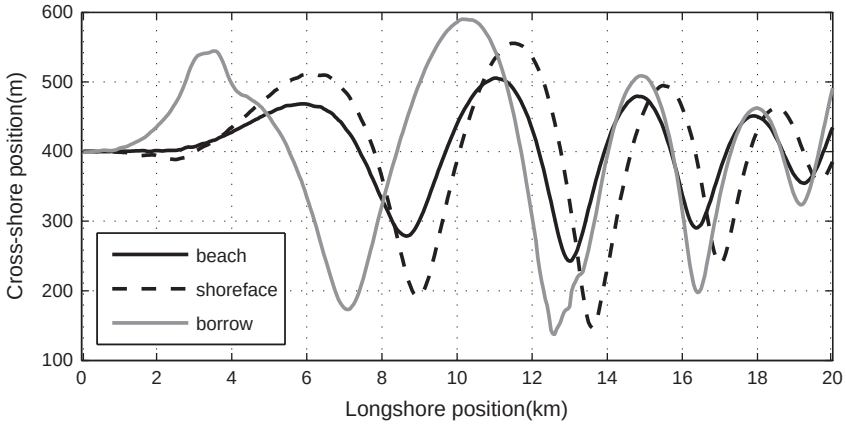

Fig. 5. Final shoreline after 8 years for the three nourishment scenarios and the default offshore wave conditions. Notice the exaggeration in the cross-shore axis.

and the generation of the downdrift sand wave train. During the second phase the domain was saturated with sand waves and σ increased only due to the growth in amplitude. During this second phase σ increased at the same constant rate for all 3 scenarios and this suggests that the behaviour of the sand wave train does not depend on the initial perturbation. Because the borrow pit scenario reached the second phase relatively fast, the amplitude of the sand wave train got bigger than for the other scenarios at the same moment in time. Fig. 6 also illustrates that for the beach nourishment scenario σ first decreased and that only after diffusion in cross-shore direction had occurred the instability slowly started to develop.

Fig. 7 shows the initial forcing of the shoreline for the shoreface nourishment and borrow pit scenarios. The refraction over the shoreface nourishment forced two erosional zones at the outer sides of its shadow and two accretional zones at the inner sides of its shadow. The accretional zones merged and grew to a single sand wave crest. This initial forcing is qualitatively in accordance with van Duin et al. (2004). The downdrift erosional zone grew and triggered the development of a downdrift sand wave train. The refraction over the borrow pit caused a mirrored forcing on the shoreline with two accretional zones at the outer sides of the shadow and an erosional zone in its shadow. Notice that this pattern does not seem realistic, when compared with most of the studies discussed at the end of Section 2. However, it is similar to what Bender and Dean (2004) found for simulations with $K_2 = 0$. In our simulations, $K_2 = K_1$ but the alongshore gradients in wave height were very small so that the second term of CERC was negligible (which is equivalent to $K_2 = 0$).

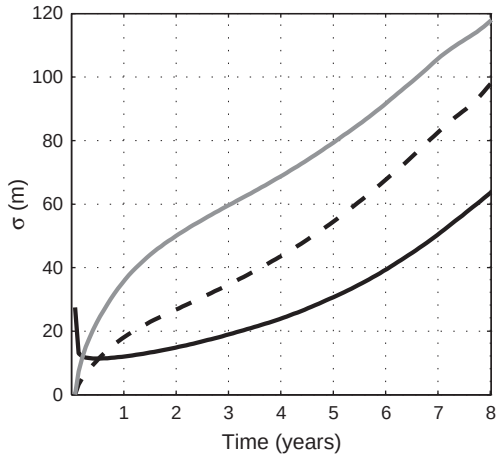

Fig. 6. Time evolution of the standard deviation of the shoreline using the default offshore wave conditions for the beach nourishment case (black solid line), the shoreface nourishment case (black dashed line) and the dredge pit case (grey solid line).

Because the borrow pit was located at deep water it was hardly filled in with sediment. Therefore its forcing on the shoreline remained relatively constant during the simulation and the first accretional zone grew in amplitude without migrating downdrift. Downdrift, the feedback mechanism took over and the erosional trough and the second accretional zone did not only grow but also migrated and a downdrift sand wave train was triggered. Notice that this is the only scenario where the second sand wave originated directly from the forcing and this contributed to the relatively fast development of the sand wave train and its larger amplitudes.

5.3. Dependence on the wave conditions

The dependence of the shoreline evolution on the offshore wave conditions can be seen in Fig. 8, which shows the standard deviation of the shoreline after 5 years for the shoreface nourishment scenario and the different wave conditions. As expected, using the default wave height and period, the coastline was stable for simulations with θ_0 lower than $\theta_{cr} = 42°$ and the corresponding shoreline variability remained low. For θ_0 greater than θ_{cr} a shoreline sand wave field developed and the variability increased, reaching a maximum of 93 m for $\theta_0 = 65°$.

The simulations with $H_0 = 0.5$ m showed a smaller σ, which increased more linearly with θ_0. Downdrift sand waves did not develop and the increase in variability was due to an increase of the amplitude of the initial perturbation. The shoreline was stable because D_c moved onshore and θ_{Dc} was lower than θ_{cr}. The amplitude of the shoreline perturbation in the shadow of the shoreface nourishment could grow to a large amplitude because the shoreface nourishment was located offshore of D_c where it was hardly diffused. The simulations with $H_0 = 1.5$ m, $T_p = 4$ s and $T_p = 8$ s caused the model to crash before the end of the simulation for θ_0 higher than 50°. Therefore only the simulations at $\theta_0 = 50°$ are compared. The simulation with $H_0 = 1.5$ m resulted in a relatively small crest for the first sand wave, which migrated downdrift and diffused slowly. This can be explained by the fast diffusion of the shoreface nourishment. The downdrift sand waves however grew and migrated at a higher rate leading to higher variability. The effect of wave height is threefold: a) it controls the position of D_c and thereby θ_{Dc} and the potential for instability, b) it affects the rate of alongshore transport and therefore the rate of sand wave development, and c) since it controls the position of the D_c, it controls the rate of the diffusion of the shoreface nourishment.

The simulation with $T_p = 4$ s resulted in a variability larger than the default simulation because the amplitude of the first sand wave was bigger and the growth of the downdrift sand waves was faster. The reason for the stronger instability is that shorter waves refract less and this leads to a relatively larger θ_{Dc}. The simulation with $T_p = 4$ s had

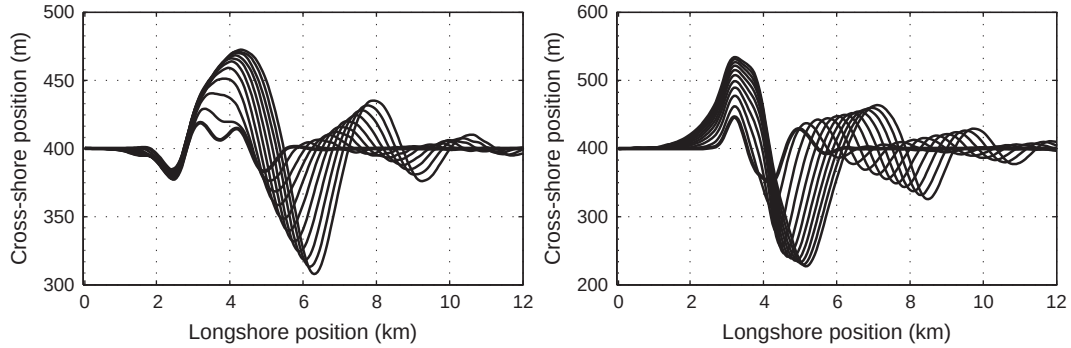

Fig. 7. Initial development of the shoreline for the shoreface nourishment scenario (left panel) and the borrow pit scenario (right panel) using the default offshore wave conditions. The shoreline is plotted every 3 months and the final line corresponds to the result after 2 years. Notice the exaggeration in the cross-shore axis.

the same variability as the simulation with $H_0 = 1.5$ m. However the amplitude of the downdrift sand waves was smaller and the equal variability was only caused by the relatively large amplitude of the first sand wave for $T_p = 4$ s. The simulation with $T_p = 8$ s resulted in a lower variability because the instability was less strong and a shoreline sand wave train with smaller amplitudes developed.

5.4. From diffusion to instability

In order to understand the physics behind the behaviour of the shoreline, simulations with the alternative model setups were performed for the beach nourishment scenario using diffusive ($\theta_0 = 40°$) and unstable conditions ($\theta_0 = 60°$) (Fig. 9). In setup A, the alongshore gradients of θ_b and H_b were both artificially disconnected. This is equivalent to the traditional one-line approach, where the gradients in alongshore transport only result from the changes in orientation of the shoreline. Setup D is the full dynamical approach of the Q2D-Morfo model. In setup B only the gradients in H_b were disconnected and in setup C only the gradients in θ_b were disconnected. For all simulations an initial rapid retreat of the shoreline of 60 m took place during the first month. This was due to the initial adaptation of the cross-shore slope of the nourishment to the slope of the equilibrium profile. After this, the diffusion in cross-shore direction became weaker and the shoreline evolution was dominated by alongshore transport. The characteristics of the nourishment development for the different setups are presented in Table 4.

The left panel of Fig. 9 shows simulations for diffusive coastline conditions ($\theta_0 = 40°$). Setup A led to a symmetrical diffusion of the perturbation. In setup B there was relatively less diffusion because waves at breaking had lower incidence angles due to refraction over curvilinear contours. Since the waves arrived obliquely, the refraction pattern around the perturbation was not symmetrical and this resulted in an asymmetrical diffusion of the perturbation, as found by Thevenot and Kraus (1995). In setup C there was more accretion on the downdrift flank of the perturbation compared to setup B and the crest moved downdrift about 400 m. For setup D, the diffusion was relatively low due to the combined effect of refraction and wave energy spreading and focusing. The perturbation showed the same asymmetrical shape but with a steeper downdrift flank. The crest of the perturbation moved downdrift about 400 m.

The right panel in Fig. 9 shows the simulations for unstable conditions ($\theta_0 = 60°$). Model setups A, B and C showed the same trends as described for stable conditions. The diffusion was however relatively lower because the more oblique waves refracted stronger up to breaking resulting in more wave energy spreading and thus a lower H_b. Moreover, setup C showed a new feature: a downdrift erosional zone with an amplitude of 1.5 meters and an alongshore width of 3 km. The downdrift erosional zone is a feature commonly observed in nature (Inman, 1987). Finally model setup D showed a completely different behaviour. The diffusion of the nourishment stopped after 55 meters of shoreline retreat. The crest of the perturbation migrated downdrift 700 m and the perturbation was asymmetric with a steeper downdrift slope. Downdrift, an erosional zone developed with an amplitude of 18 m. Further downdrift a new crest and erosional zone seemed to develop. This shows that only the combined effect of θ_b and H_b results into shoreline instability.

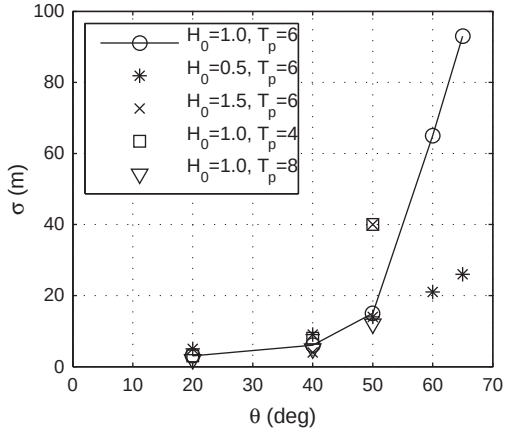

Fig. 8. Standard deviation of the final shoreline after 5 years for the shoreface nourishment case using different offshore wave conditions.

6. Discussion

6.1. Mechanism for sand wave train formation

High angle wave instability as described by Ashton and Murray (2006a) and Falqués and Calvete (2005) can be seen as a temporal instability. In their approach a shoreline sand wave field develops in unison from random initial perturbations due to the feedback between shoreline changes and the wave field. In the present study, a solitary sand wave forms due to the same feedback process but starting from a localised perturbation. Subsequently, the solitary sand wave can trigger the formation of a downdrift sand wavetrain. This latter process can be seen as a spatial-temporal instability, i.e., the growth of the perturbation both in space and time, which is a well known process in fluid dynamics. Spatial-temporal instabilities have not been described previously in coastal morphodynamics but an example from river morphodynamics can be found in Federici and Seminara (2003), who studied the generation of large-scale bedforms in rivers.

A sand wave train can only develop when the bathymetric extension of the shoreline perturbation reaches a water depth where the angle of wave incidence is larger than the critical angle,

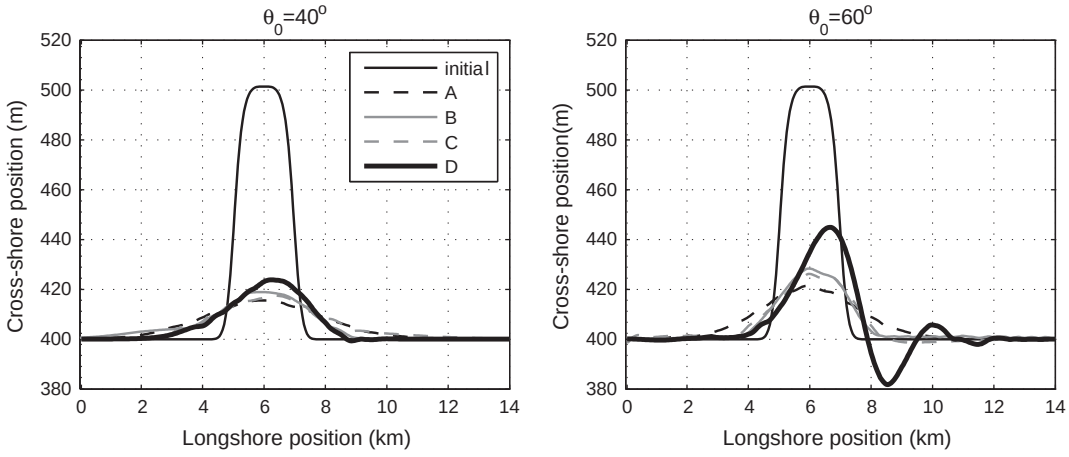

Fig. 9. Shoreline after 1 year for the beach nourishment scenario and different combinations of alongshore constant and variable values of θ_b and H_b as an input for the transport computation: A) θ_b = constant, H_b = constant, B) θ_b = variable, H_b = constant, C) θ_b = constant, H_b = variable, D) θ_b = variable, H_b = variable. Simulation A is equivalent to the traditional 1-line approach and simulation D is the most realistic approach. The left panel represents stable conditions ($\theta_0 = 40°$) and the right panel unstable conditions ($\theta_0 = 60°$). Notice the exaggeration in the cross-shore axis.

D_{cr}. If D_{cr} is greater than the depth of closure, D_{cr} cannot be reached and the coastline remains stable. This was previously suggested by List and Ashton (2007), who stated that if waves already refract below the critical angle before reaching the bathymetric perturbation, it seems unlikely that the instability effect is possible. Accordingly, the present study shows that if the shoreline perturbation initially does not extend until D_{cr} the perturbation diffuses in the cross-shore and alongshore directions. Due to cross-shore diffusion, the perturbation propagates offshore in the bathymetric lines. If this process continues until the perturbation reaches D_{cr}, instability can develop.

When the perturbation reaches D_{cr}, the pattern of the gradients in alongshore transport changes reversing the behaviour of the shoreline perturbation from diffusion to growth. Subsequently this increases the offshore extension of the perturbation and the strength of the instability. At this moment, the minimum in transport is located at the downdrift slope. The increasing transport downdrift of this location leads to the development of an erosional trough. The development of the trough is strengthened by wave focusing on its downdrift slope. Up to here, the feedback between the shoreline changes and the wave field results into the growth and migration of a solitary sand wave. However, downdrift of the trough the transport decreases to normal values leading to accretion. If this new shoreline perturbation grows and diffuses in the cross-shore direction, it may in turn feedback into the wave field, triggering the growth of a second sand wave. This chain reaction continues forming a shoreline sand wave train and can be seen as a self-organisation mechanism of the shoreline. The sand waves seem to develop with an initial wavelength in the order of 2 km.

Table 4
Shoreline characteristics after 1 year for the beach nourishment scenario and different combinations of constant and variable values of θ_b and H_b as an input for alongshore transport computation. Simulation A is equivalent tothe traditional 1-line approach and simulation D is the most realistic approach.

		A) θ_b = const. H_b = const.	B) θ_b = var. H_b = const.	C) θ_b = const. H_b = var.	D) θ_b = var. H_b = var.
$\theta_0 = 40$	Retreat	85 m	80 m	82 m	76 m
	Shape	Symmetrical	Asymmetrical	Asymmetrical	Asymmetrical
	Migration	No	No	400 m	400 m
	Instability	No	No	No	No
$\theta_0 = 60$	Retreat	79 m	72 m	74 m	55 m
	Shape	Symmetrical	Asymmetrical	Asymmetrical	Asymmetrical
	Migration	No	No	400 m	700 m
	Instability	No	No	No	Yes

6.2. Evolution of the aspect ratio and saturation

Contrary to Ashton and Murray (2006a) the aspect ratio of the simulated sand waves in the present study did not attain a fixed value. The total amplitude of the sand waves increased faster than the wavelength, although at the end of the default simulation the increase in aspect ratio seemed to slow down. Since longer simulations are not available it remains unclear how the aspect ratio would evolve further.

A stabilising mechanism not included in our model is the wave shadow effect (Ashton and Murray, 2006a). Wave shadowing is relevant for features that have large aspect ratios or that are very asymmetrical with a steep downdrift slope. In the default simulation of the present study θ_0 was equal to 60° which means that the angle of the downdrift slope should be larger than 30° to be able to create a shadow zone. If refraction of the wave rays is taken into account the angle of the shoreline should be even larger. In our simulations the maximum downdrift slope is about 10°. Therefore wave shadowing cannot be a relevant stabilising mechanism for our simulations.

In our default simulations we used an exceptional situation with only high angle waves, although on most natural coasts there is a combination of both high and low angle waves. Varying θ_0 between high and low angles during a simulation would lead to alternating stable and unstable conditions (Ashton and Murray, 2006a). During stable conditions the shoreline perturbations undergo diffusion. Depending on the relative contribution of stable and unstable waves the growth of shoreline instabilities might be dampened or even inhibited. As a preliminary test we did a simulation where θ_0 was alternated every simulated week between 60° and 40° (Fig. 10). The simulation was able to run for a longer period than our default simulations. Clearly, the instability was dampened by the low angle waves. The nourishment developed into a shoreline sand wave with a finite amplitude of about 20 m. The wavelength reached 13 km and continued to increase. A downdrift crest developed but a real sand wave train seemed not to be able to develop. This suggests that the instability mechanism does not necessarily lead to the growth of a well developed sand wave field but it could also explain the downdrift migration of more subtle shoreline undulations that maintain more or less their volume.

There are many observations of coastlines where large scale shoreline perturbations neither diffuse nor grow and only migrate

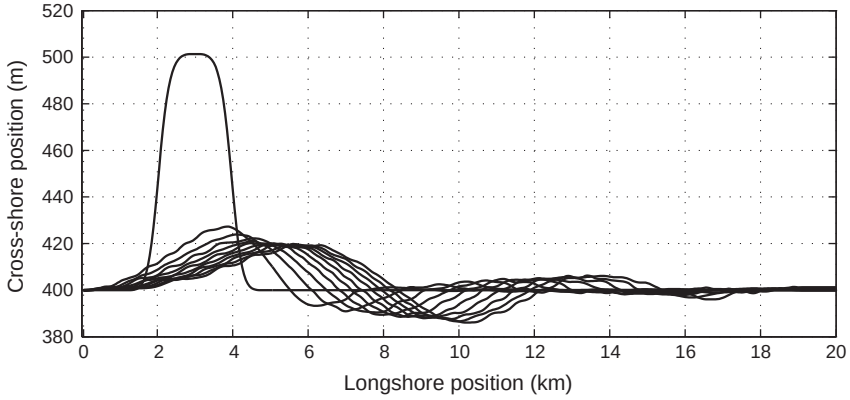

Fig. 10. Time evolution of the shoreline for the beach nourishment scenario with default wave height and period but weekly alternating wave angles of 60° and 40° (even contribution of unstable and stable conditions). The shoreline is plotted every 2 years and the final line corresponds to the result after 20 years. Notice the exaggeration in the cross-shore axis.

downdrift maintaining more or less their shape for decades. In particular, the observations of a migrating solitary shorelines and wave with a downdrift erosional trough (Inman, 1987), show resemblance to the simulation presented in the previous paragraph. Other observations show a series of sand waves (alternating accretional and erosional zones) migrating downdrift on a coastal stretch (Davidson-Arnott and van Heyningen, 2003; Ruessink and Jeuken, 2002). Even though the generation of these sand waves have been related to periodic inputs of sand, the authors suggested that HAWI could play a role in their downdrift migration and their constant volume. The previously presented simulation complements this hypothesis and provides an explanation for the finite amplitude of these observed sand wave fields. In future research it would be interesting to study in more detail the effect of variable wave conditions and chronology and to try to predict the evolution of observed sand waves.

6.3. Sand wave migration for low wave incidence angles

In the previous section it was suggested that a mixture of high and low angle waves could provide an explanation for both the formation and migration of finite amplitude sand waves. However there are many coasts dominated by low wave incidence angles (so that HAWI cannot play a role) where observations show diffusing shoreline sand waves that still migrate downdrift (Grove et al., 1987; Thevenot and Kraus, 1995). The migration of shoreline sand waves under such conditions has been explained in the past as a collective movement of sediment (Sonu, 1968) and has been modelled with one-line models by including an empirical advection term (Inman, 1987; Thevenot and Kraus, 1995). However, no physical background for this advection term has been presented. In Section 5.4 the model results show that, even for wave incidence angles below θ_{cr} (stable conditions), the feedback between the shoreline and the wave field can lead to downdrift migration of shoreline sand waves at several hundred meters per year. The numerical experiments showed that the direct effect of refraction leads to a reduced and asymmetrical diffusion and that it is the indirect effect on H_b that leads to migration. This implies that migration and diffusion can occur at the same time. The effect of wave energy spreading and focusing might therefore provide a mechanism for downdrift migration of shoreline sand waves under low angle conditions.

7. Conclusions

Simulations with a non-linear morphodynamic model indicate that a beach nourishment on a long sandy beach with waves coming predominantly from high angles could lead to the formation of a shoreline sand wave train due to high angle wave instability. The beach nourishment initially develops into a solitary shoreline sand wave, with an accretional crest and an erosional trough. Subsequently, this sand wave initiates the growth of a downdrift shoreline sand wave train. A shoreface nourishment and a borrow pit cause an indirect shoreline perturbation in their shadow and a relatively fast development of a sand wave train, which leads to larger shoreline features.

The sand wave train characteristics do not depend on the nourishment location and dimensions. Its formation is a self-organised response of the morphodynamic system and can be seen as a spatial-temporal instability. While new sand waves are formed downdrift with initial wavelengths in the order of 2 km, the amplitude and wavelength of the older sand waves increase and they migrate downdrift at a rate of hundreds of meters per year.

High angle wave instability results from the feedback of nearshore bathymetric changes to the wave field, which leads to an alongshore variation in the wave angle and height at breaking (H_b), the latter occurs due to wave energy spreading and focusing. Only if the bathymetric perturbations extend to a depth where the wave angle is greater than the critical angle, 42°, the variations in H_b lead to transport gradients that allows for growth of the perturbation. Cross-shore dynamics therefore play an important role in the development and strength of the shoreline instability. Furthermore, a coastline is potentially unstable when the wave incidence angle at the depth of closure (θ_{Dc}) is larger than 42°, which is in contrast with Ashton et al. (2001) who used the angle in deep water as a criterion. The instability is stronger for short period waves (less refraction occurs and θ_{Dc} is larger) and for higher waves (the depth of closure moves offshore and θ_{Dc} is also larger). In case of a mixture of high and low angle waves, the latter have a damping effect on the coastline instability and the beach nourishment develops into a more subtle solitary sand wave with a constant amplitude and a downdrift sand wave train hardly develops.

On a coast dominated by low wave incidence angle the feedback of the shoreline changes to the wave field can still be essential for the prediction of the evolution of nourishments. This feedback results in a lower diffusion rate than would be predicted by traditional one-line shoreline models and the gradients of H_b could result in downdrift migration of the shoreline perturbation if a prevailing transport direction is present. The latter is a commonly observed behaviour of shoreline sandy features for which no satisfactory explanation had been provided previously.

Acknowledgements

This research has been funded by the Spanish Ministerio de Educacion e Innovación by research grant CTM2009-11892/IMNOBE and a FPI scholarship for the first author within the research grant CTM2006-08875/MAR.

References

Ashton, A., Murray, A.B., 2006a. High-angle wave instability and emergent shoreline shapes: 1. modeling of sand waves, flying spits, and capes. J. Geophys. Res. 111, F04011. doi:10.1029/2005JF000422.

Ashton, A., Murray, A.B., 2006b. High-angle wave instability and emergent shoreline shapes: 2. wave climate analysis and comparisons to nature. J. Geophys. Res. 111, F04012. doi:10.1029/2005JF000423.

Ashton, A., Murray, A.B., Arnault, O., 2001. Formation of coastline features by large-scale instabilities induced by high-angle waves. Nature 414, 296–300.

Bender, C.J., Dean, R.G., 2004. Potential shoreline changes induced by three-dimentional bathymetric anomalies with gradual transitions in depth. Coast. Eng. 51, 1143–1161.

Benedet, L., List, J.H., 2008. Evaluation of the physical process controlling beach changes adjacent to nearshore dredge pits. Coast. Eng. 55, 1224–1236.

Capobianco, M., Hanson, H., Larson, M., Steetzel, H., Stive, M., Chateluse, Y., Aarninkhof, S., Karambas, T., 2002. Nourishment design and evaluation: applicability of model concepts. Coastal Eng. 47, 113–135.

Davidson-Arnott, R.G.D., van Heyningen, A., 2003. Migration and sedimentology of longshore sandwaves, Long Point, Lake Erie, Canada. Sedimentology 50, 1123–1137.

Dean, R.G., 2002. Beach nourishment. Theory and practice. World Scientific, Singapore.

Falqués, A., 2003. On the diffusivity in coastline dynamics. Geophys. Res. Lett. 30 (21), 2119. doi:10.1029/2003GL017760.

Falqués, A., Calvete, D., 2005. Large scale dynamics of sandy coastlines. Diffusivity and instability. J. Geophys. Res. 110 (C03007). doi:10.1029/2004JC002587.

Falqués, A., Calvete, D., Ribas, F., 2011. Shoreline instability due to very oblique wave incidence: Some remarks on the physics. J. Coastal Res. 27 (2), 291–295. doi:10.2112/JCOASTRES-D-09-00095.1.

Federici, B., Seminara, G., 2003. On the convective nature of bar instability. J. Fluid Mech. 487, 125–145.

Grove, R.S., Sonu, C.J., Dykstra, D.H., 1987. Fate of a massive sediment injection on a smooth shoreline at san onofre, california. Coastal Sediments 1987: Am. Soc. of Civ. Eng. , pp. 531–538.

Grunnet, N.M., Ruessink, B.G., 2004. Morphodynamic response of nearshore bars to a shoreface nourishment. Coastal Eng. 52, 119–137.

Hamm, L., Capobianco, M., Dette, H.H., Lechuga, A., Spanhoff, R., Stive, M.J.F., 2002. A summary of European experience with shore nourishment. Coastal Eng. 47, 237–264.

Hartog, W.M., Benedet, L., Walstra, D.R., van Koningsveld, M., Stive, M.J.F., Finkl, C.W., 2008. Mechanisms that influence the performance of beach nourishment: a case study in Delray Beach, Florida, U.S.A. J. Coast. Res. 24, 13041319.

Inman, D.L., 1987. Accretion and erosion waves on beaches. Shore Beach 55 (3/4), 61–66.

Komar, P.D., 1998. Beach Processes and Sedimentation, 2nd Edition. Prentice Hall, Englewood Cliffs, N.J.

List, J.H., Ashton, A.D., 2007. A circulation modeling approach for evaluating the conditions for shoreline instabilities. Coastal Sediments 2007. ASCE, pp. 327–340.

List, J.H., Hanes, D.M., Ruggiero, P., 2006. Predicting longshore gradients in alongshore transport: comparing the cerc formula to delft3d. Coastal Eng. 2006. World Scientific, pp. 3370–3380.

List, J.H., Benedet, L., Hanes, D.M., Ruggiero, P., 2008. Understanding differences between delft3d and empirical predictions of alongshore sediment transport gradients. Coastal Eng. 2008. World Scientific, pp. 1864–1875.

Ozasa, H., Brampton, A.H., 1980. Mathematical modelling of beaches backed by seawalls. Coastal Eng. 4, 47–63.

Pelnard-Considère, R., 1956. Essai de theorie de l'evolution des formes de rivage en plages de sable et de galets. 4th Journees de l'Hydraulique. : Les Energies de la Mer, Paris, Vol. III(1). Société Hydrotechnique de France, pp. 289–298.

Ruessink, B.G., Jeuken, M.C.J.L., 2002. Dunefoot dynamics along the Dutch coast. Earth Surf. Process. Land. 27, 1043–1056.

Sonu, C.J., 1968. Collective movement of sediment in littoral environment. Coastal Eng. 1968: Am. Soc. of Civ. Eng. , pp. 373–400.

Thevenot, M.M., Kraus, N.C., 1995. Longshore sandwaves at Southampton Beach, New York: observations and numerical simulation of their movement. Mar. Geol. 126, 249–269.

van Duin, M.J.P., Wiersma, N.R., Walstra, D.J.R., van Rijn, L.C., Stive, M.J.F., 2004. Nourishing the shoreface: observations and hindcasting of the Egmond case, The Netherlands. Coast. Eng. 51, 813–837.

Work, P.A., Rogers, W.E., 1997. Wave transformation for beach nourishment projects. Coastal Eng. 32, 1–18.

Zenkovich, V.P., 1959. On the genesis of cuspate spits along lagoon shores. J. Geol. 67, 269–277.